Copper and Zinc Binding Modulates the Aggregation and Neurotoxic Properties of the Prion Peptide PrP106−126[†]

Michael F. Jobling,[‡,§] Xudong Huang,[||] Leanne R. Stewart,[‡] Kevin J. Barnham,[⊥] Cyril Curtain,[#] Irene Volitakis,[‡] Matthew Perugini,[@] Anthony R. White,[‡] Robert A. Cherny,[‡] Colin L. Masters,[‡] Colin J. Barrow,[§] Steven J. Collins,[‡] Ashley I. Bush,[‡,||] and Roberto Cappai*,[‡]

Department of Pathology, The University of Melbourne, Victoria 3010, Australia, The Mental Health Research Institute, Parkville Victoria 3052, Australia, School of Chemistry, The University of Melbourne, Victoria 3010, Australia, Laboratory for Oxidation Biology, Genetics and Aging Unit, Massachusetts General Hospital East, Building 149, 13th Street, Charlestown, Massachusetts 02129, Biomolecular Research Institute, 343 Royal Parade, Parkville 3052, Australia, School of Physics, Monash University, Clayton Victoria 3168, Australia, and Department of Biochemistry and Molecular Biology, The University of Melbourne, Victoria 3010, Australia

Received December 21, 2000

ABSTRACT: The abnormal form of the prion protein (PrP) is believed to be responsible for the transmissible spongiform encephalopathies. A peptide encompassing residues 106−126 of human PrP (PrP106−126) is neurotoxic in vitro due its adoption of an amyloidogenic fibril structure. The Alzheimer's disease amyloid β peptide (Aβ) also undergoes fibrillogenesis to become neurotoxic. Aβ aggregation and toxicity is highly sensitive to copper, zinc, or iron ions. We show that PrP106−126 aggregation, as assessed by turbidometry, is abolished in Chelex-100-treated buffer. ICP-MS analysis showed that the Chelex-100 treatment had reduced Cu^{2+} and Zn^{2+} levels approximately 3-fold. Restoring Cu^{2+} and Zn^{2+} to their original levels restored aggregation. Circular dichroism showed that the Chelex-100 treatment reduced the aggregated β-sheet content of the peptide. Electron paramagnetic resonance spectroscopy identified a 2N1S1O coordination to the Cu^{2+} atom, suggesting histidine 111 and methionine 109 or 112 are involved. Nuclear magnetic resonance confirmed Cu^{2+} and Zn^{2+} binding to His-111 and weaker binding to Met-112. An N-terminally acetylated PrP106−126 peptide did not bind Cu^{2+}, implicating the free amino group in metal binding. Mutagenesis of either His-111, Met-109, or Met-112 abolished PrP106−126 neurotoxicity and its ability to form fibrils. Therefore, Cu^{2+} and/or Zn^{2+} binding is critical for PrP106−126 aggregation and neurotoxicity.

A large body of data strongly suggests Creutzfeldt-Jakob disease, bovine spongiform encephalopathy, and other transmissible spongiform encephalopathies (TSEs)[1] are caused by prions (*1*). The infectious agent is believed to consist entirely of the prion protein (PrP) and is devoid of nucleic acid. Prion biogenesis is associated with the normal cellular PrP molecule (PrP^{C}) undergoing structural change into an abnormal disease-causing conformation (PrP^{Sc}, PrP^{res}, or PrP^{TSE}). Spectroscopic studies have shown that the conversion from PrP^{C} to PrP^{TSE} results in a reduction in α-helix content from 40% in PrP^{C} to 30% in PrP^{TSE} and an increase in β-sheet content from 3% in PrP^{C} to 43% in PrP^{TSE} (*2*). A synthetic peptide encompassing human PrP residues 106−126 is highly fibrillogenic and toxic to neurons in vitro (*3*−*6*). PrP106−126 represents a suitable model peptide for studying PrP^{TSE}-mediated cell death since it shares with PrP^{TSE} the absolute requirement of PrP^{C} expression for neurotoxicity (*6*, *7*). The peptide exhibits a pH-dependent structural plasticity by undergoing a β-sheet to random coil transformation (*6*, *8*, *9*). This transformation, along with its amyloidogenic propensity, appears to be regulated by the hydrophobic core sequence (AGAAAAGAVV) from position 113 to 122 (*6*). The core region sequence from position 113 to 120 (AGAAAAGA) is necessary but not sufficient for a neurotoxic effect (*10*). Reducing the hydrophobicity of this region abolished toxicity which correlated with a reduction in its aggregation and fibril forming properties (*6*).

PrP106−126 shares a number of biophysical properties with the Alzheimer's disease amyloid β peptide (Aβ). There is a good correlation between Aβ toxicity and its physicochemical properties (*11*−*14*). Aβ residues 25−35 are similar to the hydrophobic core sequence of PrP106−126, and have an important role in stabilizing the Aβ aggregates that induce

[†] This work is supported by National Health and Medical Research Council of Australia Grant 114212 and Australian Research Council Grant S0004973.

* To whom correspondence should be addressed. Phone: (+61-3) 8344-5882. Fax: (+61-3) 8344-4004. E-mail: r.cappai@unimelb.edu.au.

[‡] Department of Pathology, The University of Melbourne, and The Mental Health Research Institute.

[§] School of Chemistry, The University of Melbourne.

[||] Massachusetts General Hospital East.

[⊥] Biomolecular Research Institute.

[#] Monash University.

[@] Department of Biochemistry and Molecular Biology, The University of Melbourne.

[1] Abbreviations: Aβ, amyloid β protein; CD, circular dichroism; DMSO, dimethyl sulfoxide; ESI, electrospray ionization; ICP-MS, inductively coupled plasma mass spectrometry; IDA, iminodiacetate; NMR, nuclear magnetic resonance; EPR, electron paramagnetic resonance; PrP, prion protein; TSE, transmissible spongiform encephalopathy.

10.1021/bi0029088 CCC: $20.00
Published on Web 06/16/2001

neurotoxicity. Amino acid residues from Gly-33 to Met-35 modulate Aβ neurotoxicity (*14*), while the two valines at positions 39 and 40 affect its β-sheet stability (*15*). Importantly, not all peptides which form a β-sheet structure, such as aggregated islet amyloid protein (*16*) and glucagon (*17*), are toxic. This indicates that additional factors besides secondary structure are necessary for toxicity. There is a growing body of data which demonstrate that transition metals are an isogenous factor that modulate Aβ aggregation and toxicity (*18*). Copper, iron, and zinc promote Aβ aggregation into amyloidogenic aggregates (*19*−*21*). The interaction between Aβ and Cu^{2+} results in copper reduction and the generation of hydrogen peroxide (*22*). This effect is sequence specific since rat Aβ, which differs from the human form in three residues, binds these metals with a lower affinity and is less susceptible to metal-induced aggregation than human Aβ. Furthermore, the different length Aβ species associated with AD interact differently with these metals (*23*). The Aβ42 species, the level of which is elevated in familial AD, has a higher affinity for these metals, resulting in an increased level of aggregation and a higher level of hydrogen peroxide production compared to those of the shorter Aβ40 species. The aggregation of Aβ could be inhibited by adding a metal chelator to the aggregation environment (*20*, *23*). The physiological relevance of this effect is strongly supported by the ability of metal chelators to increase the level of solubilization of Aβ from Alzheimer's disease brains (*24*). A role for copper in PrP106−126 toxicity is suggested by the copper chelator bathocuprionic sulfonate inhibiting PrP106−126 toxicity (*25*).

Given the critical role transition metals have in the biophysical behavior and activity of Aβ, this study investigated whether this property is common to other amyloidogenic peptides, by studying the effect of metals on PrP106−126 aggregation. In this paper, we show that fibrillization of PrP106−126 was completely inhibited in an environment depleted of transition metals. Cu^{2+} and to a lesser extent Zn^{2+} could restore PrP106−126 aggregation. The metal binding site was localized and found to comprise the N-terminal amino group, His-111, and Met-112.

MATERIALS AND METHODS

Materials. Peptide coupling reagents and amino acids were purchased from Auspep Pty. Ltd. (Melbourne, Australia). Dimethylformamide (DMF) was stored over 4 Å sieves for 48 h to remove water and dimethylamine. Peptide synthesis resins were from Calbiochem-Novabiochem. Anhydrous hydrogen fluoride (HF) was obtained from CIG Gases. Copper-coated carbon grids and uranyl acetate was purchased from ProSciTech. All other chemicals were purchased from Sigma or Aldrich Chemical Co.

Peptide Synthesis. PrP106−126 and its analogues were synthesized by manual Boc chemistry protocols (*26*) or by automated solid-phase Fmoc flow chemistry on a Biolynx Crystal instrument. 2-(1*H*-Benzotriazol-1-yl)-1,1,3,3-tetramethyluronium hexafluorophosphate (HBTU), 1-hydroxybenzotriazole (HOBt), and diisopropylethylamine (DIEA) were used as activators of carboxylic residues. Fmoc-synthesized peptides were cleaved from the solid support by a trifluoroacetic acid (TFA)/1,2-dithioethane (EDT)/triethylsilane (TES)/water (92.5:2.5:2.5:2.5) mixture over the course of 2 h. Boc-synthesized peptides were cleaved by an anhydrous HF/*p*-cresol (9:1) mixture over the course of 90 min. All crude peptides were precipitated in ether and filtered through 10 mL of Sephadex G-25 size-exclusion resin to remove any scavengers and salts formed during the cleavage procedure. Peptides were then injected into a Beckman HPLC system equipped with a PDA detection system, using an aqueous acetonitrile gradient. A Zorbax C8 semipreparative column was used. Peptide purity was confirmed by RP-HPLC; amino acid analysis and LC−ESI-MS were performed on a Micromass triple-quadrupole mass spectrometer equipped with a Hewlett-Packard 1100 liquid chromatography pump system. Purity was greater than 95% for all the peptides that were used.

Metal-Depleted and Metal-Supplemented Buffer Preparation. Chelex-100-treated phosphate buffer solutions (10 mM) were prepared by suspending Chelex-100 resin in 50 mL of 10 mM phosphate buffer and stirring for 24 h. Metal-supplemented "synthetic" buffers were made from the Chelex-100-treated phosphate buffer (10 mM) to which the appropriate amounts of metal had been added. The metals were added in the form of $CuCl_2$, $ZnCl_2$, $CoCl_2$, $MnCl_2$, and $AlSO_4$. The final metal concentrations were measured by ICP-MS.

Aggregation Assay. Stock solutions were prepared by dissolving 2.0 mg of each peptide in 300 μL of dimethyl sulfoxide (DMSO). The peptide solution was then sonicated for 20 min in a water bath and filtered through a 0.22 μm filter (Millipore). Aliquots of stock peptide solutions were added to aqueous buffer [10 mM phosphate (pH 7.4)] to a final volume of 1 mL and a final peptide concentration of 20 μM. Metal concentrations of the buffers were as stated. Samples contained no more than 0.5% DMSO. Final solutions were placed in a 1 mL acryl cuvette (Sarstedt) for analysis. The extent of aggregation was determined by measuring turbidity at 400 nm versus a buffer blank. The peptide solutions were briefly vortexed before each absorbance measurement to suspend any particulate matter. Delay times were calculated by extrapolating the steepest portion of each aggregation curve to zero absorption (*27*).

Circular Dichroism (CD). Circular dichroism studies were performed on an Aviv 62DS spectropolarimeter at 25 °C. A 0.1 cm quartz cell was used for spectra recorded from 190 to 250 nm. Samples contained 100 μg/mL peptide in 10 mM potassium phosphate buffer (pH 7.3).

Electron Microscopy. Peptide solutions from aggregation assays were vortexed to suspend the particulate matter, and a 5 μL aliquot was spotted onto carbon-coated copper grids (ProSciTech). The grids were allowed to air-dry and the fibrils negatively stained with 0.5% uranyl acetate for 3 min and then washed several times with water. The samples were analyzed on a Siemens ELMISKOP 102 electron microscope at 60 eV.

Analytical Ultracentrifugation. A Beckman Optima model XL-A analytical ultracentrifuge equipped with a photoelectric absorbance optical detection system was used for all sedimentation experiments. Samples (100 μL) and reference (120 μL) solutions were loaded into a conventional double-sector filled Epon centerpiece (path length of 1.2 cm) with quartz windows and mounted in a Beckman An-60 Ti rotor. Data were collected at 235 nm with three averages at time intervals of 30 min and radial intervals of 0.001 cm until sedimentation equilibrium was attained. Experiments were

conducted at 20 °C with rotor velocities of 40 000 and 60 000 rpm. The partial specific volume of PrP106−126 (0.7448 $cm^3\ g^{-1}$) was calculated from the amino acid composition (*28*). Solvent densities were computed using the program SEDNTERP (*28*), kindly supplied by D. Hayes (Magdalen College, Durham, NC), T. Laue, and J. Philo (Alliance Protein Laboratories, Thousand Oaks, CA). Estimates of the weight-average molar mass (M_w) were obtained from the global nonlinear least-squares best fit to sedimentation equilibrium data at both speeds, using the program SEDEQ1B (kindly supplied by A. Minton, National Institutes of Health, Bethesda, MD), according to

$$A(r) = A(r_0)\exp^{[(\omega^2/2RT)M_w(1-\nu\rho)(r^2-r_0^2)]} + E \qquad (1)$$

where $A(r)$ is the absorbance at radius r, $A(r_0)$ the absorbance at the reference radius r_0, ω the rotor angular velocity, R the gas constant, T the temperature, M_w the weight-average molar mass, ν the partial specific volume of the solute, ρ the solvent density, and E the baseline offset.

High-Performance Immobilized Metal Ion Affinity Chromatography. High-Performance immobilized metal ion affinity chromatography (HP-IMAC) was performed by a modified literature method (*28*, *29*) as previously described (*30*). HiTrap chelating Sepharose cartridges (Amersham-Pharmacia) were mated to a Beckmann HPLC system unit comprising a System Gold programmable solvent module (model 126), a diode array detector module (model 168), and a rheodyne injector. The peptide was eluted with a pH gradient from pH 7.3 to 4.0 using buffer A [20 mM potassium phosphate containing 0.5 M NaCl (pH 7.3)] and buffer B [20 mM potassium phosphate containing 0.5 M NaCl (pH 4.0)]. Peptides were freshly prepared in buffer A and acetonitrile (90:10). The column was equilibrated with buffer A and charged with a 0.1 M solution of either $CuCl_2$, $NiCl_2$, or $ZnCl_2$ in buffer A until saturation was achieved. The excess metal ions were removed by a single wash of 5 mL with distilled water, and the column was re-equilibrated with buffer A. The peptide was eluted with a gradient of 100% buffer A to buffer B over the course of 15 min at a rate of 1 mL/min. Between runs, the column was removed, regenerated by washing manually with copious amounts of distilled water, 50 mM EDTA, and distilled water, and then re-equilibrated in buffer A.

Inductively Coupled Plasma Mass Spectrometry (ICP-MS) for Analysis of Metal Concentrations. Samples were diluted in a 1% HNO_3 solution for analysis by ICP-MS. ICP-MS was performed using an Ultramass 700 instrument (Varian, Victoria, Australia) in peak-hopping mode with spacing at 0.100 amu, 1 point/peak, 50 scans/replicate, 3 replicates/sample, and a dwell time of 10 000 μs. The rate of plasma flow was 15 L/min with an auxiliary flow of 1.5 L/min. The RF power was 1.2 kW. The sample was introduced using a glass nebulizer at a flow rate of 0.88 L/min. The apparatus was calibrated using a 1% HNO_3 solution containing Cu and Zn at 5, 10, 50, and 100 ppb with Y39 being the internal standard for all isotopes of Cu and Zn.

Nuclear Magnetic Resonance (NMR) Spectroscopy. NMR samples were prepared by dissolving the lyophilized peptides in 500 μL of 10 mM phosphate buffer (pH 6.9) and 50 μL of ^2H_2O. The pH was adjusted with small additions of 0.5 M NaO^2H or ^2HCl. The metal concentrations of the samples were increased by the addition of 0.1 M $CuCl_2$ and $ZnCl_2$. The ^1H chemical shifts were referenced to 2,2-dimethyl-2-silapentane-5-sulfonate (DSS) at 0 ppm, via the chemical shift of the H_2O resonance (*32*).

Spectra were recorded on a Bruker AMX-500 spectrometer. Most spectra were recorded at 298 K, with probe temperatures calibrated according to the method of van Geet (*33*). Solvent suppression was achieved by pulsed field gradients using the WATERGATE method of Piotto et al. (*34*). Spectra were processed using XWINNMR, version 1.3 (Bruker), and analyzed using XEASY [version 1.3.13 (*35*)]. Sine-squared window functions, phase shifted by 60−90°, were applied in both dimensions prior to Fourier transformation.

Electron Paramagnetic Resonance (EPR) Spectroscopy. X-Band EPR spectra of the Cu^{2+}−peptide complexes were obtained using a Bruker EC106 spectrometer. Samples (25 μL) were drawn into 100 μL micropipets and handled as described by Gordon and Curtain to ensure reproducibility (*36*). The sample temperature was maintained at 110 K using a flow-through cryostat. The microwave frequency was measured using a Bruker EIP 548B frequency counter, and the magnetic field was calibrated with a sample of 1,1-diphenyl-2-picryl hydrazyl.

Neurotoxicity Assay on Mouse Cerebellar Granule Neurons. The PrP knockout mice ($PrP^{-/-}$) mice were obtained from C. Weissmann (Institut fur Molekularbiologie I, Zurich, Switzerland) (*37*). Wild-type (WT) control mice (C57BL6J × 129/Sv) with the same genetic background as the $PrP^{-/-}$ mice were chosen. Primary cultures of cerebellar granule neurons were established from the $PrP^{-/-}$ and WT mice as described previously (*6*). Briefly, cerebella from postnatal day 4−5 (P4−5) mice were removed, dissected free of meninges, and dissociated in 0.025% trypsin. Cells were then plated at a density of 350 000 cells/cm^2 onto 5 μg/mL poly(L-lysine)-coated 48-well plates (Costar) in BME supplemented with 10% FCS, 2 mM glutamine, 25 mM KCl, and gentamycin sulfate (100 μg/mL). Cultures were maintained at 37 °C in 5% CO_2. AraC (5 μg/mL) was added on day 1. The MTT assay was used to assess cell survival in all the assays. PrP106−126, PrP106−126 scrambled, H111S, M109S, and M112S peptides were freshly prepared as 1 mM stock solutions in media. On day 1, in vitro neurons were exposed to 80 μM peptide in culture medium for a period of 2 days. Fresh peptide was then added, and cell viability was measured by the MTT assay after an additional 2 days.

RESULTS

Chelex-100 Treatment Abolishes PrP106−126 Aggregation. To determine if metals modulated PrP106−126 aggregation, turbidometry was used to compare the aggregation of PrP106−126 either in normal phosphate buffer or in phosphate buffer pretreated with Chelex-100 chelating resin. As seen in Figure 1A, the aggregation of PrP106−126 was completely abolished in the Chelex-100-treated buffer. It was only after ∼120 h that a small increase in the level of aggregation in the Chelex-100 sample was detected (Figure 1A). To determine which metals were altered by the Chelex-100 treatment, the metal concentration in the normal and Chelex-100 buffers was measured by inductively coupled plasma mass spectrometry (ICP-MS). The Chelex-100 treatment caused a 4-fold reduction in Cu^{2+} concentration and a

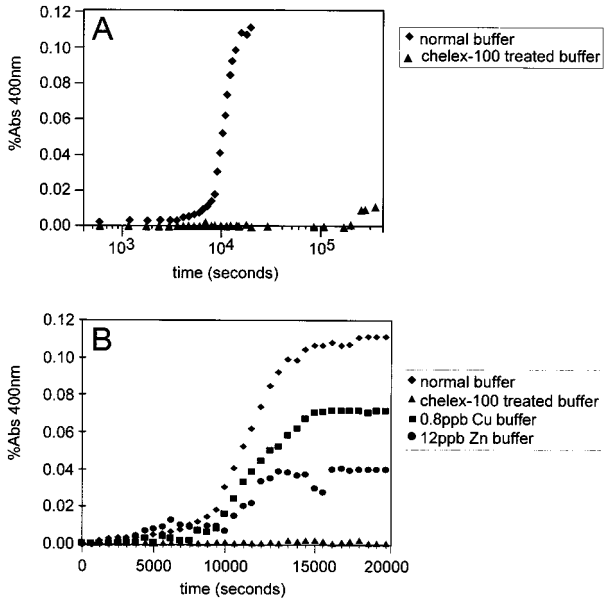

FIGURE 1: Analysis of peptide aggregation assessed by turbidometry (400 nm). (A) Aggregation of PrP106−126 in either normal (◆) or Chelex-100 (▲) buffer. The Chelex-100-treated buffer completely abolishes peptide aggregation. (B) Aggregation of PrP106−126 following the addition of copper (■) and zinc (●) to the Chelex-100 buffer to their original values. Data for aggregation of PrP106−126 in normal (◆) and Chelex-100 (▲) buffer are overlaid for comparison. Calculated lag times are given in Table 3.

Table 1: Peptide Names, Sequences, and Abbreviations Used in This Study[a]

Peptide	Peptide sequence	Abbreviation
PrP106-126	KTNMKHMAGAAAAGAVVGGLG	PrP106-126
PrP106-126 M109S	KTNMKHSAGAAAAGAVVGGLG	M109S
PrP106-126 H111S	KTNMKSMAGAAAAGAVVGGLG	H111S
PrP106-126 M112S	KTNSKHMAGAAAAGAVVGGLG	M112S
PrP106-126 M109S/M112S	KTNSKHSAGAAAAGAVVGGLG	MM/SS
PrP106-126 H111S/M109S/M112S	KTNSKSSAGAAAAGAVVGGLG	HMM/SSS
PrP106-126 C-terminally amidated	KTNMKHMAGAAAAGAVVGGLG-NH_2	amidated
PrP106-126 N-terminally acetylated and C-terminally amidated	Ac-KTNMKHMAGAAAAGAVVGGLG-NH_2	acetylated
PrP106-126 scrambled	NGAKALMGGHGATKVMVGAAA	scrambled

[a] All mutations have been introduced to alter the potential metal binding of the wild-type PrP106−126 peptide. The mutated serines are underlined. The numbering is based on the human PrP gene (*54*).

3-fold reduction in Zn^{2+} concentration (Table 2). There was no significant change in Al^{3+}, Ni^{2+}, or Mn^{2+} levels. To examine the individual effect of Cu^{2+} and Zn^{2+} on PrP106−126 aggregation, a series of synthetic buffers was made by adding Cu^{2+} or Zn^{2+}, to restore the original concentrations in the Chelex-100-treated buffer. The metal concentrations in the synthetic buffers were confirmed by ICP-MS and corresponded very closely to their normal buffer values (Table 2). The aggregation profile of PrP106−126 in these synthetic buffers was measured (Figure 1B and Table 3), and Cu^{2+} and Zn^{2+} restored aggregation to 70 and 40%, respectively, of the normal buffer levels. There was a small, but not significant, increase in the delay time (Table 3). Since neither Cu^{2+} nor Zn^{2+} alone was able to fully restore aggregation to normal buffer levels, it suggests they may act cooperatively. To test this, Cu^{2+} and Zn^{2+} were added together, and this increased the aggregation plateau height to 80% of that of the normal buffer. The failure to restore the level of aggregation to 100% suggests that some additional factor may be removed by the Chelex-100 treatment. To determine if there is a dose-dependent response, increasing concentrations of Cu^{2+} or Zn^{2+} were tested. A 2-fold increase in Cu^{2+} levels (1.6 ppb Cu) resulted in a 100% aggregation plateau height (Table 3). A 5-fold increase in Cu^{2+} concentration (4.0 ppb Cu) resulted in a 200% plateau height compared to normal buffer. Increasing Zn^{2+} concentrations displayed a much lesser effect than Cu^{2+}. Doubling the Zn^{2+} concentration (24 ppb Zn) did not change the plateau height. An 8-fold increase (100 ppb Zn) was required to obtain a 100% plateau height (Table 3). The higher Zn^{2+} levels also increased the delay time by 60% to 8000 s.

Metal Depletion Does Not Cause a Major Alteration in the Secondary Structure of PrP106−126. Circular dichroism was used to determine if the lack of PrP106−126 aggregation in the Chelex-100 buffer was due to alterations in the secondary structure of PrP106−126. The three signature wavelength absorption peaks utilized to detect secondary structure were the 195 nm minima for random coil, the 208 and 222 nm double minima for α-helix, and a single β-sheet minimum near 225 nm (*38*). PrP106−126 was analyzed in both normal buffer and Chelex-100 buffer at pH 5, 6, 7.3, and 8. The CD spectra were overall similar in both normal buffer and Chelex-100-treated buffer, and the normal buffer spectra were consistent with previous studies (data not shown) (*4*, *6*, *9*, *26*). In normal buffer at pH 7.3, PrP106−126 displayed a single minimum near 225 nm, indicating large β-sheet aggregates were present (*15*, *39*, *40*). In the Chelex-100 buffer at pH 7.3, PrP106−126 displayed a similar profile, but with a β-sheet minimum near 218 nm. This minimum is expected for soluble, low-molecular weight β-sheet structure (*38*). Therefore, the Chelex-100 treatment caused a significant reduction in aggregated β-sheet content. This would be consistent with the decreased level of aggregation of PrP106−126 in Chelex-100 buffer.

Analysis of the PrP106−126 Oligomeric State by Transmission Electron Microscopy and Analytical Ultracentrifugation. The physical structures of the aggregated peptides formed during the turbidity assay were analyzed by negatively staining the aggregated peptides with uranyl acetate and viewed by electron microscopy. The PrP106−126 peptide in normal buffer formed fibrils that were consistent with those previously reported (*4*, *6*). In contrast, the Chelex-100-treated sample was devoid of fibrils and consisted of amorphous aggregates.

To compare the oligomeric states of soluble PrP106−126 in the normal and the Chelex-100 buffers, sedimentation studies were employed in the analytical ultracentrifuge. The weight-average molar mass of PrP106−126 solubilized in normal buffer was calculated to be 1700 Da (from eq 1 in Materials and Methods), in agreement with the theoretical monomer molar mass of PrP106−126 (1912 Da). No other soluble oligomeric species were detected. However, a time-dependent reduction in optical density was observed, providing evidence for the loss of aggregated material during the

Table 2: Metal Concentrations of the Buffers Used in This Study As Determined by ICP-MS[a]

buffer	Cu^{2+} ($n = 48$)	Zn^{2+} ($n = 52$)	Mn^{2+} ($n = 38$)	Al^{2+} ($n = 37$)	Co^{2+} ($n = 22$)	Ni^{2+} ($n = 38$)
normal	0.71	11.45	1.94	19.54	0.16	1.32
Chelex-100	0.18	3.45	1.51	18.91	0.61	1.35
0.8 ppb Cu	0.81	b	b	b	b	b
12 ppb Zn	b	12.1	b	b	b	b
1.8 ppb Mn	b	b	1.86	b	b	b
19 ppb Al	b	b	b	20.3	b	b
0.8 ppb Co	b	b	b	b	0.66	b
0.8 ppb Cu and 12 ppb Zn	0.83	12.2	b	b	b	b
1.6 ppb Cu	1.68	b	b	b	b	b
24 ppb Zn	b	23.6	b	b	b	b
1.6 ppb Cu and 24 ppb Zn	1.70	23.8	b	b	b	b
4.0 ppb Cu	4.12	b	b	b	b	b
100 ppb Zn	b	99.8	b	b	b	b

[a] All values are in parts per billion. Where concentrations are not given (b), they are regarded as "baseline" and resemble those found in the Chelex-100 buffer.

Table 3: Turbidity Data for PrP106−126 in Buffers of Varying Metal Concentrations Confirmed by ICP-MS[a]

buffer	plateau height (%)	delay time (s)
normal	100	5000
Chelex-100	0	na
0.8 ppb Cu	70	5500
12 ppb Zn	40	5800
1.8 ppb Mn	0	na
19 ppb Al	0	na
0.8 ppb Co	0	na
0.8 ppb Cu and 12 ppb Zn	80	8500
1.6 ppb Cu	105	5000
24 ppb Zn	45	8000
1.6 ppb Cu and 24 ppb Zn	150	8000
4.0 ppb Cu	200	5000
100 ppb Zn	90	8000

[a] Plateau heights are measured relative to PrP106−126 in normal buffer. na, not applicable.

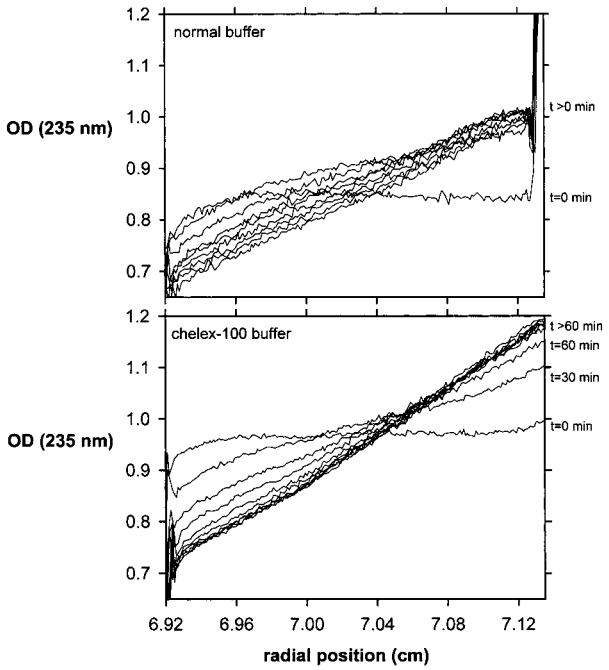

FIGURE 2: Sedimentation profiles of PrP106−126 in the presence and absence of divalent metal ions. The optical density (OD) at 235 nm is plotted as a function of radial position. The solid lines indicate the first 10 radial scans measured at 30 min intervals for PrP106−126 solubilized in 10 mM potassium phosphate (pH 7.4) and Chelex-100-treated 10 mM potassium phosphate buffer (pH 7.4). When identifiable, the scans are labeled with a time point of minutes.

course of the experiment (Figure 2). A similar phenomenon has previously been observed with human apolipoprotein C-II, which has recently been demonstrated to form amyloid in vitro (*41*). In contrast, we did not detect a significant loss in optical density with time when samples of PrP106−126 solubilized in Chelex-100-treated buffer were studied in the analytical ultracentrifuge (Figure 2). Furthermore, the weight-average molar mass of PrP106−126 in Chelex-100-treated buffer was determined to be 1910 Da, consistent with the monomeric molar mass. This indicates that the metal-depleted environment maintains PrP106−126 in a monomeric state, in agreement with the turbidity studies (Figure 1).

Measuring the Level of Metal Binding of PrP106−126 by HP-IMAC. The above data suggest that PrP106−126 binds metal ions, in particular Cu^{2+} and Zn^{2+}. To directly demonstrate this, a HP-IMAC procedure was used to measure the level of binding of PrP106−126 to Ni^{2+}, Cu^{2+}, and Zn^{2+} metal chelates (*31*). The PrP106−126 peptide was strongly retained on both the IDA−Zn^{2+} and IDA−Cu^{2+} chelates (Table 4). It was only at pH 4 that the peptide eluted from these columns, along with the metal itself. PrP106−126 displayed a weaker affinity for the IDA−Ni^{2+} chelate and eluted at approximately pH 6.5. The PrP106−126 scrambled sequence peptide had a high affinity for Cu^{2+}, a lower affinity for Ni^{2+}, and no affinity for Zn^{2+}. This demonstrates that the natural affinity of histidine for Cu^{2+} is present in both the PrP106−126 and PrP106−126 scrambled sequence peptides. However, the PrP106−126 scrambled peptide allowed differentiation between specific and nonspecific binding of PrP106−126 to Zn^{2+} since PrP106−126 scrambled did not bind Zn^{2+}, indicating Zn^{2+} binding is sequence specific. Since the PrP106−126 scrambled peptide is nontoxic and does not form fibrils and lacks any β-sheet (*26*), the natural histidine−copper interaction alone is not responsible for the amyloidogenic and toxic activity of PrP106−126.

Analysis of PrP106−126 Metal Interactions by NMR Spectroscopy. To characterize the interaction of PrP106−126 with Cu^{2+} and Zn^{2+} at the molecular level, the effects of Cu^{2+} and Zn^{2+} on the ^1H NMR spectrum of PrP106−126 were studied. A combination of two-dimensional total

Table 4: Elution pH of PrP106−126 and Mutant Analogues on Immobilized Iminodiacetiate−Metal Chelating Chromatography[a]

	IDA−Cu^{2+}	IDA−Zn^{2+}	IDA−Ni^{2+}
PrP106−126	4.0	4.0	6.5
M109S	4.0	7.3	6.5
H111S	7.3	7.3	7.3
M112S	4.0	7.3	6.5
MM/SS	4.0	7.3	6.5
MHM/SSS	7.3	7.3	7.3
amidated	4.0	7.0	7.3
acetylated	4.0	7.3	6.5
PrP106−126 scrambled	4.0	7.3	7.3

[a] Elution at pH 7.3 indicates no affinity, while at pH 4.0, both the peptide and the metal are stripped off the column, indicating high affinity. Intermediate elution at pH 6.5 indicates moderate affinity.

correlation spectroscopy and nuclear Overhauser effect spectroscopy was used to assign the ^1H resonances in the Chelex-100 buffer. Comparison between PrP106−126 in both normal and Chelex-100-treated buffer showed no difference in the spectra, confirming there were no changes in structure. The addition of either $CuCl_2$ or $ZnCl_2$ caused differential broadening of resonances, which allowed localization of the metal binding site in PrP106−126. The paramagnetic nature of Cu^{2+} affects the NMR spectra and will cause a resonance broadening on top of any resonances affected by metal interactions. The addition of 0.5 molar equiv of Cu^{2+} caused a significant broadening, to the point beyond detection, of the Hϵ (8.8 ppm) and Hδ (7.5 ppm) resonances of His-111. The addition of 1.0 molar equiv of Zn^{2+} to the peptide flattened the Hϵ (8.8 ppm) and Hδ (7.5 ppm) resonances of His-111 and caused a shift of a Met Hγ and Hϵ resonance (Figure 3). As the Met-109 and Met-112 resonances overlap in the normal buffer, it was not possible to identify the methionine affected by the addition of Zn^{2+} contributing to this change. However, it was obvious that a Met Hγ peak was lost from 2.7 ppm upon Zn^{2+} addition and that the Hϵ resonance had moved from 2.1 to 1.95 ppm. Therefore, His-111 and one of the methionines are directly affected by the binding of Zn^{2+} to PrP106−126. No other amino acid residues appeared to be affected by Zn^{2+}.

Analysis of the Interaction between PrP106−126 and Cu by EPR Spectroscopy. To overcome the limitations imposed by the paramagnetic nature of Cu^{2+} in the NMR studies, EPR was used to further define the interaction between Cu^{2+} and PrP106−126. The EPR spectra of PrP106−126 incubated with 2 molar equiv of Cu^{2+} in 10 mM phosphate buffer (pH 7.3) gave a $g_{||}$ of 2.17 G and a hyperfine splitting $A_{||}$ of 16.13 mK (Table 5). These values correlate with a two-nitrogen, two-sulfur (2N2S) or a two-nitrogen, one-sulfur, one-oxygen (2N1S1O) coordination complex (*42*). The NMR and EPR data indicate that the Met-109 and/or Met-112 amino acids contribute the sulfur ligands for Cu^{2+} binding to PrP106−126. While His-111 provides one nitrogen ligand, the source of the other nitrogen is unclear and may come from either the amide backbone or the N-terminal NH_2 group. If 2N1S1O binding is present, the oxygen ligand may originate from a backbone carbonyl group or the buffer environment.

Biophysical Properties of Methionine and Histidine Mutant Peptides. To establish the role of His-111, Met-109, Met-112, and the N-terminal amino group in PrP106−126 metal binding and aggregation, several mutant peptides were synthesized (Table 1). The histidine and methionine residues

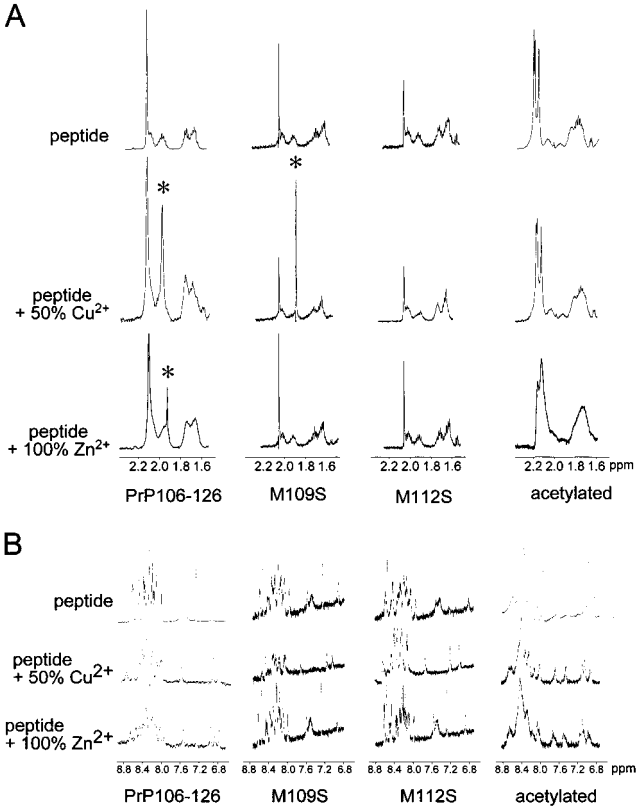

FIGURE 3: ^1H NMR spectrum of PrP106−126 and selected mutants in normal buffer (pH 7.3) and with the addition of 50% $CuCl_2$ and 100% $ZnCl_2$. (A) Aliphatic side chain region. Met-112−metal interaction peaks are marked (asterisks). (B) Amide region.

Table 5: EPR Values of $g_{||}$ and $A_{||}$ for PrP106−126 and Mutants[a]

	$g_{||}$ (G)	$A_{||}$ (mK)	coordination
PrP106−126	2.17	16.13	2N1S1O
M109S	2.11	16.25	2N1S1O
H111S	2.11	16.25	2N1S1O
M112S	2.11	16.25	2N1S1O
MM/SS	2.24	15.55	2N2O
MHM/SSS	2.24	15.55	weak 2N2O
amidated	2.11	16.25	2N1S1O
acetylated	nd	nd	very weak binding

[a] Coordination is based upon the work of Piesach and Blumberg (*42*) for natural Cu binding proteins (*41*). nd, not detected.

were changed to serine, as opposed to the more commonly used alanine, to avoid increasing the hydrophobicity of the peptide which can influence its ability to aggregate (*6*). A C-terminally amidated peptide was synthesized to study the effects of altering the dipolar moment of the peptide. An N-terminally acetylated and C-terminally amidated peptide was synthesized to assay the potential role of the N-terminal NH_2 group.

The effect of the mutations on aggregation was tested in normal buffer (Figure 4). The H111S mutation had the most dramatic effect and completely abolished aggregation. The M109S mutation had little effect, and the peptide aggregated strongly to a plateau height of 90% of that of PrP106−126 with an increase in the delay time to 7000 s. The M112S mutation had a more pronounced effect than Met-109 and reduced aggregation to 50% of the PrP106−126 plateau height. An additive effect was seen with the double-methionine mutant peptide, MM/SS, which reached a plateau

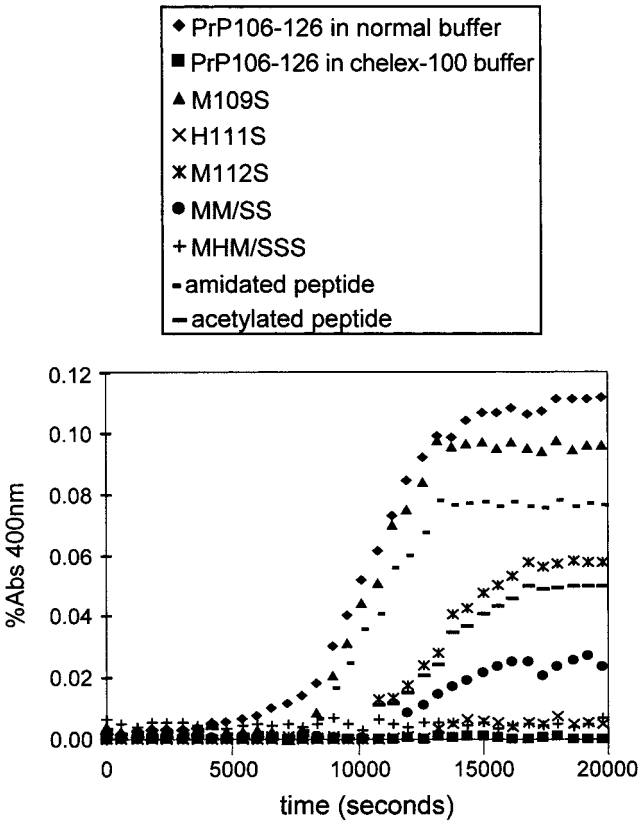

FIGURE 4: Aggregation of PrP106−126 and the mutant peptides in normal phosphate buffer (pH 7.3) as assessed by turbidometry: PrP106−126 (◆), M109S (▲), H111S (×), M112S (*), MM/SS (●), MHM/SSS (+), amidated peptide (-), and acetylated peptide (−). Data for PrP106−126 in Chelex-100 buffer (■) are overlaid for comparison.

height of only 30% of that of PrP106−126. The M112S and MM/SS peptides had longer delay times of 10 000 and 10 500 s, respectively. The triple-mutant peptide, MHM/SSS, displayed no significant aggregation. Amidating the C-terminus increased the delay time to 8000 s and reduced the aggregation plateau height to 70% of that of the wild-type peptide. The N-terminally acetylated peptide also had a longer delay time of approximately 10 000 s and only aggregated to 40% of the level of PrP106−126. When all peptides were tested in Chelex-100 buffer, no aggregation was observed (data not shown). When the mutant peptides are compared to PrP106−126, it is evident that His-111 is critical for facilitating aggregation, while Met-112 and the N-terminal amide group also have an important role in modulating the overall level of aggregation. Met-109 had a smaller effect on PrP106−126 aggregation and is presumably less critical for metal binding and the subsequent peptide aggregation.

The mutations did not alter the secondary structure of the peptides as measured by CD in normal buffer and Chelex-100 buffer at pH 7.3. All of the His and Met mutant peptides and the amidated peptide exhibited spectra very similar to those of the PrP106−126 peptide. The spectrum of the acetylated peptide in normal buffer was similar to that of PrP106−126. However, in Chelex-100 buffer, it exhibited a slight double minimum at 208 and 222 nm (data not shown). This represents a tendency of this peptide to adopt a helical configuration once the dipolar moment of the peptide has been altered significantly. Previous work has shown PrP106−126 readily becomes helical in the presence of trifluoroethanol (TFE) (*26*, *43*). The physical structure of the mutant peptides formed during the turbidity assays was analyzed by transmission electron microscopy. All of the mutants formed amorphous particulate clusters, and no fibrillogenic species could be detected (Figure 5). Therefore, while M109S was able to aggregate strongly, it could not form fibrils.

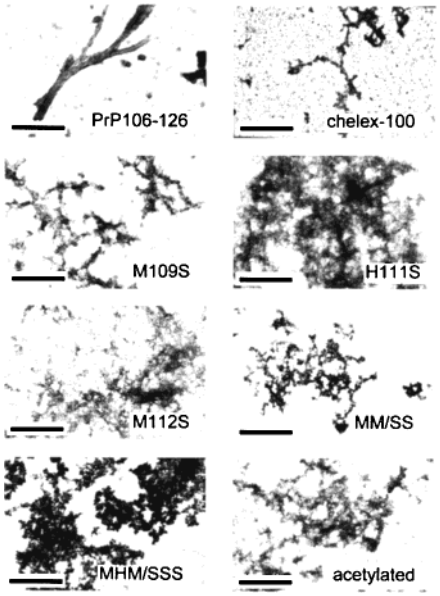

FIGURE 5: Transmission electron micrographs of PrP106−126 and the mutant peptides after negative staining with uranyl acetate. The scale bar is equal to 50 nm.

The metal binding properties of the mutant peptides for Ni^{2+}, Cu^{2+}, and Zn^{2+} metal chelates was measured by HP-IMAC (Table 4). Only the amidated peptide bound to the IDA−Zn^{2+} chelate, but was readily eluted at pH 7.0, implying a weak affinity. The other mutant peptides had no measurable level of binding to Zn^{2+}. All the peptides that contained His-111 eluted at pH ∼4, indicating a high-affinity binding to the IDA−Cu^{2+} chelate due to the naturally strong affinity of histidine for Cu^{2+}. However, PrP106−126 had the longest retention time on the column, suggesting it had the highest affinity for Cu^{2+}. The H111S and MHM/SSS peptides showed no affinity for Cu^{2+} and did not bind to the IDA−Cu^{2+} column. All the Cu^{2+}-binding peptides also displayed a mild affinity for Ni^{2+} and eluted at pH ∼6.5.

The mutant peptides were analyzed by NMR, with and without Cu^{2+} or Zn^{2+} added. The addition of 0.5 molar equiv of Cu^{2+} caused all the His-111-containing peptides (M109S, M112S, and MM/SS) to experience His peak broadening, like wild-type PrP106−126. The His Hϵ and Hδ resonances of M109S were no longer visible. Peptide M112S showed the His Hδ resonance had moved from 7.6 to 7.4 ppm and had no visible His Hγ peak. The MM/SS peptide had the His Hδ resonance shift from 7.45 to 7.3 ppm, and the His Hϵ resonance was still present at 8.8 ppm. The MHM/SSS peptide exhibited a loss of the Lys-106 backbone chain amide resonance with Cu^{2+}. The H111S peptide showed no further resonance changes in this region. Analysis of the Met Hγ and Hϵ region (1.8−2.5 ppm) following Cu^{2+} addition showed that only the M109S peptide was affected (Figure 3). The overlapping Met peaks at 2.3 ppm are now smaller, and a new peak at 2.2 ppm had formed. No other mutant peptides experienced this change. The addition of Zn^{2+} to

the His/Met mutant peptides caused no significant peak broadening or relocations to occur. The addition of Cu^{2+} to the N-terminally acetylated peptide gave results similar to those for the mutant peptides with broadening of the His resonances. The addition of Zn^{2+} did not alter the Met peaks and only caused a slight reduction in the signal intensity of the His imidazole resonance.

EPR analysis of the mutant peptides, under the same conditions that were used for PrP106−126, showed that the spectrum of the amidated peptide, M109S, and M112S are essentially identical with a $g_{||}$ of 2.11 G and a hyperfine splitting $A_{||}$ of 16.25 mK (Table 5). These values deviate from those of the wild-yype PrP106−126 binding complex, yet still are evidence of maintenance of a 2N1S1O coordination sphere about Cu^{2+}. While no 2N1S1O binding region was identified in natural Cu binding proteins (*42*), it is feasible that such binding occurs and would have $g_{||}$ and $A_{||}$ values located midway between those for 2N2S and 2N2O binding. However, no literature reports utilizing EPR of such a complex could be found to confirm that this occurs. The MM/SS mutant gave a spectrum markedly different from those of the other peptides with a $g_{||}$ of 2.24 G and a hyperfine splitting $A_{||}$ of 15.55 mK. This is consistent with a 2N2O coordination to Cu^{2+}. The H111S and MHM/SSS peptides gave very weak EPR spectra and required an up to 3-fold increase in Cu^{2+} levels to achieve the spectrum of the copper-bound peptide. This large excess of Cu^{2+} gave a weak spectrum for H111S and MHM/SSS with $g_{||}$ and $A_{||}$ values of 2.11 G and 16.25 mK and 2.24 G and 15.55 mK, respectively. Theses values indicate a possible 2N1S1O coordination for H111S and 2N2O coordination for MHM/SSS. The acetylated peptide showed very weak binding to Cu^{2+}. The NMR and EPR studies on the mutant peptides confirm that both His-111 and the N-terminal amino group are crucial for Cu^{2+} binding, while Met-112 rather than Met-109 directly participates in this binding. Without His-111, the Cu^{2+} ion may be coordinated, albeit very weakly, to the N-terminus as seen with the acetylated peptide.

Mutagenesis of His-111, Met-109, or Met-112 Abolishes PrP106−126 Neurotoxicity. Since the histidine and methionine mutations altered the metal binding and aggregation properties of the peptides, the effect of these mutations on their neurotoxic activity was assayed on mouse cerebellar granular neuronal cultures from both normal and $PrP^{-/-}$ mice. As expected, PrP106−126 caused a 30% decrease ($p < 0.05$) in WT neuronal survival after 4 days (Figure 6), but had not effect on the $PrP^{-/-}$ neurons, confirming specificity for PrP-expressing neurons (*6*, *7*). All the mutant peptides showed no significant toxicity against WT neurons. These data demonstrate that the metal binding residues appear to simultaneously modulate the ability of the peptide to form fibrils and be neurotoxic.

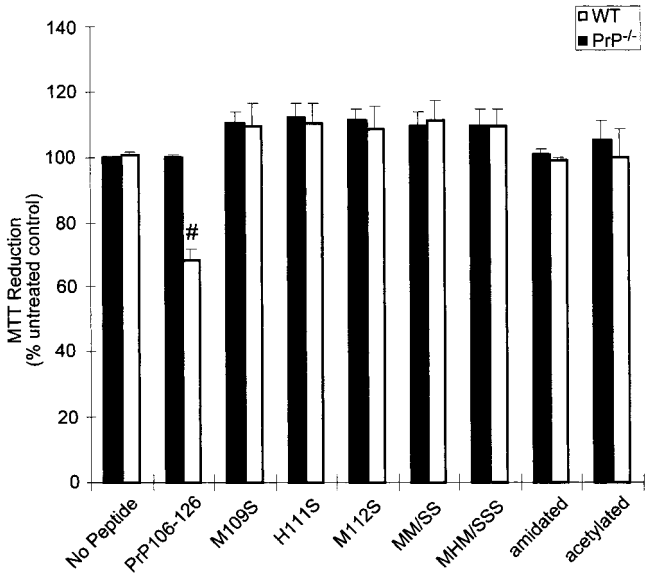

FIGURE 6: Neurotoxicity assays of PrP106−126 and the mutant peptides on primary cerebellar neurons from wild-type and $PrP^{-/-}$ mice. Cells were treated with 80 μM peptide for 4 days, and cell viability was determined by the MTT assay. Mean neurotoxicity values are the average of five independent experiments ($n = 5$) performed in triplicate for each treatment. Error bars represent ± standard deviation. Statistical significance was determined by an ANOVA test [$p < 0.05$ (#)].

DISCUSSION

The main finding of this work is that the N-terminal polar region of the neurotoxic PrP106−126 peptide contains a metal binding site for Cu^{2+} and Zn^{2+} which modulates aggregation and toxicity. The reduction in Cu^{2+} levels following Chelex-100 treatment abolished its fibrillogenic propensity without causing major alterations in its secondary structure. In concert with the results using various mutant peptides, metal binding is not responsible for forming β-sheet structure in PrP106−126 (*4*, *6*). The combination of NMR, EPR, and mutagenesis experiments showed that His-111 was crucial for copper binding, along with the N-terminal amino group and Met-112.

The aggregation profile of PrP106−126 is consistent with a highly amyloidogenic peptide, similar to the Aβ peptide of Alzheimer's disease (*27*, *44*). Aggregation is composed of an initial lag phase followed by the growth phase which reaches a plateau beyond which no further aggregation occurs. The lag phase is believed to involve seed or nucleus formation. The seeds then form protofibrils, and these extend into the fibrils during the growth phase. The plateau height measures the overall level of aggregation. In metal-depleted buffer, PrP106−126 aggregation is completely abolished, and only restored when copper or zinc is reintroduced. The transmission electron micrographs demonstrated there was no fibril formation in the Chelex-100 buffer. Therefore, Cu^{2+} or Zn^{2+} is necessary for proper fibril polymerization to occur. Cu^{2+} and Zn^{2+} appear to act cooperatively since simultaneously restoring both metals to their normal levels results in an additive effect. However, the inability of Cu^{2+} or Zn^{2+} either alone or in combination to fully restore aggregation suggests some other, unidentified, factor has been removed by the Chelex-100. These studies do not clarify whether the role of Cu^{2+} and Zn^{2+} is in seed or protofibril formation. The data clearly indicate that in addition to the hydrophobic region, which is responsible for forming a β-sheet core (*6*), the binding of Cu or Zn is critical for aggregation. Although PrP106−126 could also bind Ni^{2+}, albeit weakly, the Chelex-100 treatment abolished aggregation without altering Ni^{2+} levels, indicating Ni^{2+} is not directly involved in the aggregation process.

The spectroscopic and biochemical studies on the wild-type and mutant peptides identified a 2N1S1O coordination for Cu^{2+} binding, with His-111 as the key residue together

with Met-112 and the N-terminal amino group. Turbidometry data indicate Met-109 is not important for peptide aggregation, but the TEM and cell culture assays demonstrate Met-109 is a necessary residue for fibril formation and neurotoxicity. The aggregation reaction is also sequence specific since the PrP106−126 scrambled peptide which bound Cu^{2+}, via the natural affinity of histidine for Cu^{2+}, does not form fibrils and is not neurotoxic. Therefore, it is the combination of a specific peptide sequence combined with its metal binding activity that leads to fibrillization and the generation of neurotoxic PrP106−126.

His-111 is the key residue for metal binding and aggregation since its replacement had the most profound effect by completely abolishing aggregation. The H111S peptide was unable to bind to the Cu^{2+}−IDA column, and as determined by EPR, there was very weak Cu^{2+} binding presumably via the N-terminal amino group. The different behavior of the methionine mutant peptides, M109S and M112S, indicated the methionine residues had distinct effects on Cu^{2+} binding and peptide aggregation. The M109S peptide had aggregation properties very similar to those of PrP106−126, whereas M112S had a much slower and lower level of aggregation. Although Met-112 has a more prominent role in Cu^{2+} binding than Met-109, the finding that the MM/SS peptide aggregated less than M112S indicates Met-109 also plays a role probably as a secondary or alternate sulfur ligand. This is consistent with the EPR spectra showing a 2N1S1O system. Interestingly, when Met-112 was not present, the EPR values indicate a shift toward a 2N2O system, while still remaining in the 2N2S boundaries of the natural Cu binding proteins (*39*). The oxygen ligands could be from the serine residue that has been mutated into the sequence or from the peptide backbone, most probably from the carbonyl group of Met-112. Alternatively, this could represent a 2N1S1O system with a water molecule bound to the metal. Peptidylglycine monoxygenase binds to copper in this coordination, although it has not been previously defined by EPR and requires further investigation (*45*). Metal binding was also modulated by the N-terminal amino group since acetylating the N-terminus caused a lower overall level of aggregation, presumably by disrupting binding of Cu^{2+} to PrP106−126.

The NMR data show direct evidence for Zn^{2+} binding to PrP106−126 but not to any of the mutant peptides. NMR data are consistent with Zn^{2+} coordinating PrP106−126 in a fashion similar to that of Cu^{2+}, so a 2N1S1O binding would also be applicable for the PrP106−126−Zn complex. The key residues identified so far, His-111 and Met-112, both experience identical peak loss or movement in the NMR spectrum, when compared to the data for the PrP106−126−Cu complex. His-111 does not have the same natural affinity for Zn^{2+} that it does for Cu^{2+}, and the overall level of binding to Zn^{2+} by the peptide is therefore lower. The mutation of any one of the identified metal binding residues abolishes Zn^{2+} binding, indicating each has a crucial role to play in Zn binding as opposed to that seen with the Cu^{2+} experiments.

On the basis of our experimental evidence, we have proposed a model for the binding of Cu^{2+} to PrP106−129 as shown in Figure 7A. The EPR data indicate that the predominant configuration about Cu^{2+} is square planar with a 2N1S1O coordination sphere. The NMR data clearly show that the imidazole side chain of His-111 is one of the ligands, while the lack of interaction between Cu^{2+} and Ac-PrP106−126 is evidence that the N-terminal amino group of the peptide is also required for metal binding. Mutagenesis and aggregation data implicate the sulfur of M112. However the NMR data are somewhat equivocal; if the sulfur of M112 was bound to copper, it would be expected that the resonance due to $C^{\epsilon}H_3$ of M112 would be broadened beyond detection. The NMR data actually show that this resonance is shifted (marked with asterisks in Figure 4), and this suggests that this residue is in a different chemical environment but not directly bound to Cu^{2+}. We have no direct evidence of the nature of the oxygen ligand, which could be solvent H_2O, phosphate from the buffer, or a backbone carbonyl from the peptide. In light of the NMR evidence, we propose that the oxygen ligand is the carbonyl from M112; this would explain the observed changes in the NMR spectrum. If the M112 that is coordinated to the Cu^{2+} is from another peptide (intermolecular coordination as shown in Figure 7A) to create an oligomeric form of the peptide, the effect of this type of coordination may not be observed in the NMR as the faster relaxation of higher-order aggregates coupled with the paramagnetic nature of copper leads to a broadening of resonances. A consequence of this is that NMR does not observe the major product from the reaction. However, these types of oligomers would be observed by EPR which would not be influenced by the effect on relaxation time of higher-order polymers or aggregates. Line broadening of the EPR spectra due to Heisenberg exchange was not observed, indicating that the Cu^{2+} centers in any polymers or aggregates were well separated, as indicated in panels A and B of Figure 7. The formation initially of metal-mediated dimers acts as a seeding event that brings the hydrophobic AGAAAAGAVV region of the two peptides into proximity such that they can stack together in a "steplike" arrangement facilitating chain extension and fibril formation.

In comparison to the PrP106−126 metal binding site, the N-terminal octapeptide repeats of PrP bind up to four copper atoms via histidine residues and possibly glycine residues (*46*, *47*). Several different models for the PrP octapeptide−Cu complex have been proposed. The first binding coordination proposed incorporated a 2N2O square planar system (*48*). This peptide−copper complex was bound by the N_{π} atom from the imidazole side chain in histidines of two adjacent repeat units and by the carbonyl groups of two glycine residues. Another model showed a 3N1O binding site which suggested binding occurs via the N_{π} atom from the histidine together with two deprotonated main chain amide nitrogens from the triglycines (*49*). NMR and EPR studies led to a tetragonal coordination indicative of a 3N1O coordination site (*46*). A four-octarepeat peptide would coordinate the four copper ions with nitrogens from the histidine imidazole group from two adjacent repeats and a nitrogen from the amide backbone. The final ligand, an oxygen molecule, is most likely from water. A two-octarepeat peptide would involve a similar arrangement (*46*). The most recent study, using EPR and CD spectroscopy, demonstrated that both the 3N1O systems (*46*, *49*) exist in equilibrium (*50*). At pH 7.45, it was shown that the model of Miura et al. (*49*) is the major binding mode, while the model of Viles et al. (*46*) is also present and can bind Cu^{2+} (*50*). Electron spin-echo envelope modulation spectra demonstrate that the

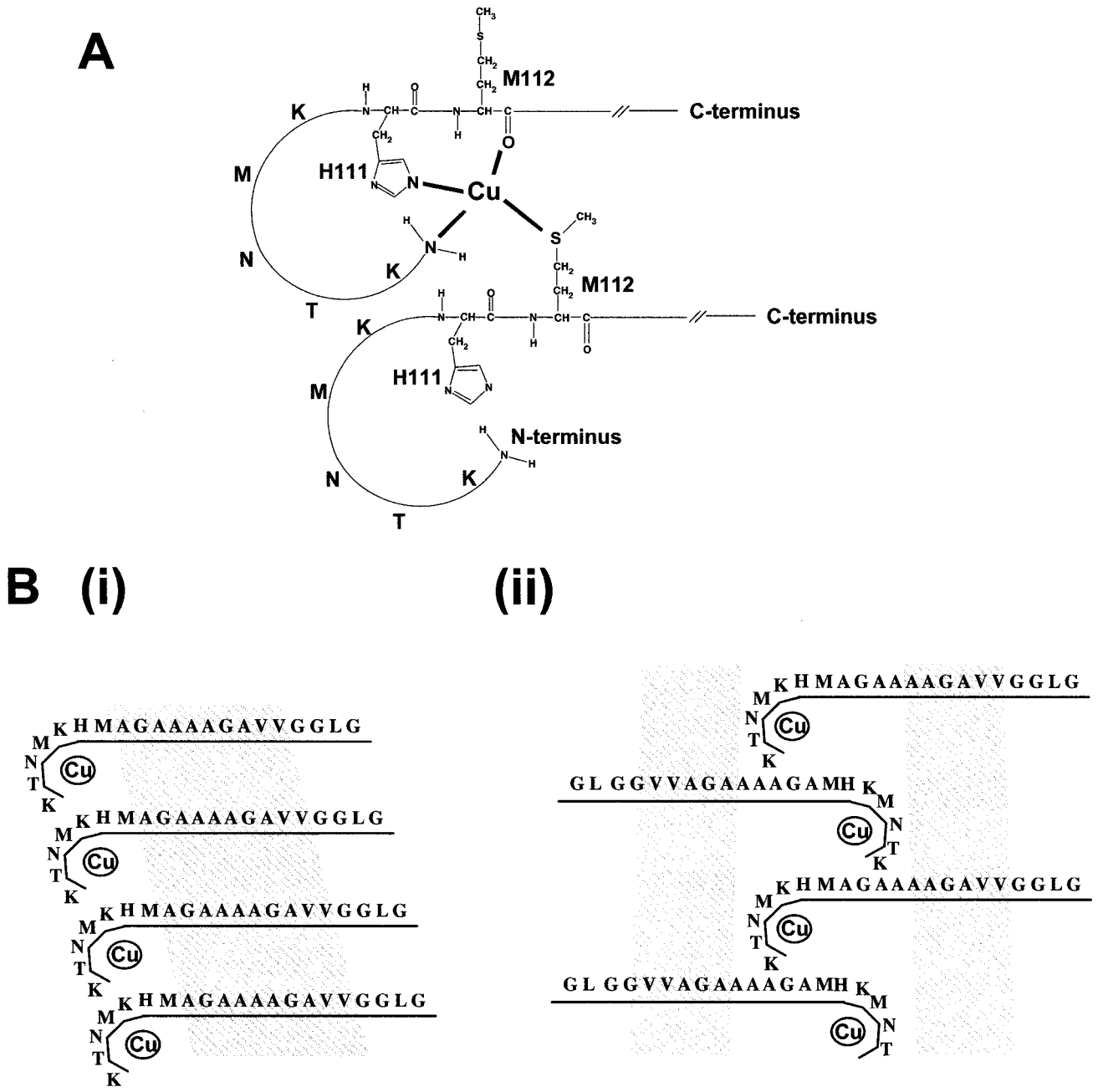

FIGURE 7: (A) Hypothetical model based upon the EPR data showing a 2N1S1O coordination complex for Cu with two molecules of PrP106−126. The side chains for His-111 and Met-112 are given in detail. The N- and C-terminal ends of the peptide are shown, and the sequence of the peptide is represented in single-letter code. (B) Schematic model showing possible PrP106−126 hydrophobic core stacking (cross-hatched) in both a parallel β-sheet (i) and an antiparallel β-sheet arrangement (ii).

histidine imidazole nitrogen contributes a nitrogen coordination site. Interestingly, EPR and CD studies on a truncated repeat unit (HGGGW) yielded spectra identical to that of a single full repeat sequence peptide in the 3N1O (histidine imadazole, glycine amide, and glycine amide) orientation described above (*50*). This would then represent a single binding unit and suggests that inter-repeat unit metal binding is not necessary and may not occur.

A recent study of PrP106−126 also identified His-111 as a crucial residue since a histidine to alanine mutation reduced the extent of fibril formation (*43*, *51*), and therefore correlates with the present findings. However, in contrast to our studies, this mutation, as well as a histidine to lysine mutation, did not alter the overall aggregation propensity of the peptide (*51*). Met-112 was also found to be important for aggregation. This is of potential biological relevance as the human PrP109−122 sequence can induce sheet structure in human PrP104−122 but not in the corresponding mouse peptide (*52*). It has also been shown that oxidizing the Met-112 sulfur lowers the sheet-forming tendency of PrP109−122 (*52*). This could be explained by it altering the affinity of the sulfur for metal ions.

PrP106−126 neurotoxicity on wild-type cells expressing PrP^C is regulated by available copper (*25*). Addition of up to 100 μM bathocuprine sulfonate inhibits nearly 80% of the observable toxicity. The hydrophobic core sequence AGAAAAGA is required for toxicity but is not solely sufficient to invoke a toxic response (*10*). These data are in agreement with our own findings, i.e., that aggregation is modulated by the hydrophobic core and the metal bind-

ing site and this in turn is necessary for PrP106−126 neurotoxicity.

The current studies have shown that the fibrillogenic and neurotoxic activity of PrP106−126 is modulated by metals in a manner similar to that described for the Aβ peptide (*19*−*22*, *31*). Aβ can bind Cu^{2+}, Fe^{2+}, and Zn^{2+} in vitro, each accelerating Aβ aggregation. Aβ aggregation is also inhibited by adding a metal chelator to the buffer (*23*). The interaction between Aβ and Cu^{2+} or Fe^{2+} results in redox chemistry due to the Aβ being a redox-active peptide that can reduce Cu^{2+} to Cu^{+} and Fe^{3+} to Fe^{2+}. In the presence of oxygen, this leads to hydrogen peroxide production (*22*). Zn^{2+} binding to Aβ appears to be protective since it inhibits Aβ-mediated Cu^{2+} reduction and hydrogen peroxide production, simultaneously protecting cells against Aβ toxicity (*53*). Unlike the Aβ peptide, PrP106−126 cannot reduce Cu^{2+} (X. Huang and A. I. Bush, unpublished observations), indicating this redox-active process is not shared by all neurotoxic amyloidogenic peptides.

We have shown that PrP106−126, a peptide model for PrP^{Sc} toxicity, interacts with metals to form neurotoxic amyloidogenic structures. While the PrP106−126 sequence does not appear to be present in PrP-associated plaques as a unique entity, the PrP106−126 metal binding sequence could participate in metal binding in vivo and perhaps modulate PrP^{TSE} structure and toxicity. Therefore, testing the possible role of this site in full-length PrP warrants further investigation. Since PrP106−126 toxicity requires PrP^{C} expression, copper binding to the peptide may promote the interaction between the PrP106−126 and PrP^{C}.

ACKNOWLEDGMENT

We thank Anna Friedhuber for assistance with electron microscopy and Geoff Howlett for access to and advice with the analytical ultracentrifuge. We thank Andy Hill, James Thyer, and Konrad Beyreuther for helpful discussions.

REFERENCES

1. Prusiner, S. B. (1998) *Proc. Natl. Acad. Sci. U.S.A. 95*, 13363−13383.
2. Pan, K. M., Baldwin, M., Nguyen, J., Gasset, M., Serban, A., Groth, D., Mehlhorn, I., Huang, Z., Fletterick, R. J., Cohen, F. E., and Prusiner, S. B. (1993) *Proc. Natl. Acad. Sci. U.S.A. 90*, 10962−10966.
3. Forloni, G., Angeretti, N., Chiesa, R., Monzani, E., Salmona, M., Bugiani, O., and Tagliavini, F. (1993) *Nature 362*, 543−546.
4. Tagliavini, F., Prelli, F., Verga, L., Giaccone, G., Sarma, R., Gorevic, P., Ghetti, B., Passerini, F., Ghibaudi, E., Forloni, G., Salmona, M., Bugiani, O., and Frangione, B. (1993) *Proc. Natl. Acad. Sci. U.S.A. 90*, 9678−9682.
5. Brown, D. R., Schmidt, B., and Kretzschmar, H. A. (1996) *Nature 380*, 345−347.
6. Jobling, M. F., Stewart, L. R., White, A. R., McLean, C., Friedhuber, A., Maher, F., Beyreuther, K., Masters, C. L., Barrow, C. J., Collins, S. J., and Cappai, R. (1999) *J. Neurochem. 73*, 1557−1565.
7. Brown, D. R., Herms, J., and Kretzschmar, H. A. (1994) *NeuroReport 5*, 2057−2060.
8. Selvaggini, C., De Gioia, L., Cantu, L., Ghibaudi, E., Diomede, L., Passerini, F., Forloni, G., Bugiani, O., Tagliavini, F., and Salmona, M. (1993) *Biochem. Biophys. Res. Commun. 194*, 1380−1386.
9. De Gioia, L., Selvaggini, C., Ghibaudi, E., Diomede, L., Bugiani, O., Forloni, G., Tagliavini, F., and Salmona, M. (1994) *J. Biol. Chem. 269*, 7859−7862.
10. Brown, D. R. (2000) *Mol. Cell. Neurosci. 15*, 66−78.
11. Pike, C. J., Walencewicz, A. J., Glabe, C. G., and Cotman, C. W. (1991) *Brain Res. 563*, 311−314.
12. Mattson, M. P., Tomaselli, K. J., and Rydel, R. E. (1993) *Brain Res. 621*, 35−49.
13. Hilbich, C., Kisters-Woike, B., Reed, J., Masters, C. L., and Beyreuther, K. (1992) *J. Mol. Biol. 228*, 460−473.
14. Pike, C. J., Walencewicz-Wasserman, A. J., Kosmoski, J., Cribbs, D. H., Glabe, C. G., and Cotman, C. W. (1995) *J. Neurochem. 64*, 253−265.
15. Barrow, C. J., and Zagorski, M. G. (1991) *Science 253*, 179−182.
16. Pike, C. J., Burdick, D., Walencewicz, A. J., Glabe, C. G., and Cotman, C. W. (1993) *J. Neurosci. 13*, 1676−1687.
17. Yankner, B. A., Duffy, L. K., and Kirschner, D. A. (1990) *Science 250*, 279−282.
18. Bush, A. I. (2000) *Curr. Opin. Chem. Biol. 4*, 184−191.
19. Bush, A. I., Pettingell, W. H., Multhaup, G., d'Paradis, M., Vonsattel, J. P., Gusella, J. F., Beyreuther, K., Masters, C. L., and Tanzi, R. E. (1994) *Science 265*, 1464−1467.
20. Atwood, C. S., Moir, R. D., Huang, X., Scarpa, R. C., Bacarra, N. M., Romano, D. M., Hartshorn, M. A., Tanzi, R. E., and Bush, A. I. (1998) *J. Biol. Chem. 273*, 12817−12826.
21. Miura, T., Suzuki, K., Kohata, N., and Takeuchi, H. (2000) *Biochemistry 39*, 7024−7031.
22. Huang, X., Cuajungco, M. P., Atwood, C. S., Hartshorn, M. A., Tyndall, J. D., Hanson, G. R., Stokes, K. C., Leopold, M., Multhaup, G., Goldstein, L. E., Scarpa, R. C., Saunders, A. J., Lim, J., Moir, R. D., Glabe, C., Bowden, E. F., Masters, C. L., Fairlie, D. P., Tanzi, R. E., and Bush, A. I. (1999) *J. Biol. Chem. 274*, 37111−37116.
23. Atwood, C. S., Scarpa, R. C., Huang, X., Moir, R. D., Jones, W. D., Fairlie, D. P., Tanzi, R. E., and Bush, A. I. (2000) *J. Neurochem. 75*, 1219−1233.
24. Cherny, R. A., Legg, J. T., McLean, C. A., Fairlie, D. P., Huang, X., Atwood, C. S., Beyreuther, K., Tanzi, R. E., Masters, C. L., and Bush, A. I. (1999) *J. Biol. Chem. 274*, 23223−23228.
25. Brown, D. R. (2000) *Biochem. J. 352*, 511−518.
26. Jobling, M. F., Barrow, C. J., White, A. R., Masters, C. L., Collins, S. J., and Cappai, R. (1999) *Lett. Pept. Sci. 6*, 129−134.
27. Evans, K. C., Berger, E. P., Cho, C. G., Weisgraber, K. H., and Lansbury, P. T., Jr. (1995) *Proc. Natl. Acad. Sci. U.S.A. 92*, 763−767.
28. Laue, T. M., Shah, B. D., Ridgeway, T. M., and Pelletier, S. L. (1992) in *Analytical Ultracentrifugation in Biochemistry and Polymer Science*, pp 90−125, The Royal Society of Chemistry, Cambridge, U.K.
29. Balakrishnan, R., Parthasarathy, R., and Sulkowski, E. (1998) *J. Pept. Res. 51*, 91−95.
30. Arnold, F. H. (1991) *Bio/Technology 9*, 151−156.
31. Liu, S. T., Howlett, G., and Barrow, C. J. (1999) *Biochemistry 38*, 9373−9378.
32. Wishart, D. S., Bigam, C. G., Yao, J., Abildgaard, F., Dyson, J., Oldfield, E., Markley, J. L., and Sykes, B. D. (1995) *J. Biomol. NMR 6*, 135−140.
33. van Geet, A. L. (1970) *Anal. Chem. 42*, 679−680.
34. Piotto, M., Saudek, V., and Sklenar, V. (1992) *J. Biomol. NMR 2*, 661−666.
35. Bartels, C., Xia, T.-H., Billeter, M., Güntert, P., and Wüthrich, K. (1995) *J. Biomol. NMR 5*, 1−10.
36. Gordon, L. M., and Curtain, C. C. (1988) in *Advances in Mebrane Fluidity* (Aloia, R. C., Curatin, C. C., and Gordon, L. M., Eds.) pp 25−89, Alan R. Liss, New York.
37. Bueler, H., Fischer, M., Lang, Y., Bluethmann, H., Lipp, H. P., DeArmond, S. J., Prusiner, S. B., Aguet, M., and Weissmann, C. (1992) *Nature 356*, 577−582.
38. Fasman, G. D. (1996) Circular Dichroism and the conformational analysis of biomolecules, in *The Language of Science* (Fasman, G. D., Ed.) Plenum Press, New York.
39. He, W., and Barrow, C. J. (1999) *Biochemistry 38*, 10871−10877.

40. Barrow, C. J., Yasuda, A., Kenny, P. T. M., and Zagorski, M. G. (1992) *J. Mol. Biol. 225*, 1079−1093.
41. Hatters, D. M., MacPhee, C. E., Lawrence, L. J., Sawyer, W. H., and Howlett, G. J. (2000) *Biochemistry 39*, 8276−8283.
42. Peisach, J., and Blumberg, W. E. (1970) *Arch. Biochem. Biophys. 165*, 691−708.
43. Ragg, E., Tagliavini, F., Malesani, P., Monticelli, L., Bugiani, O., Forloni, G., and Salmona, M. (1999) *Eur. J. Biochem. 266*, 1192−1201.
44. Jarrett, J. T., Berger, E. P., and Lansbury, P. T., Jr. (1993) *Biochemistry 32*, 4693−4697.
45. Prigge, S. T., Kolhekar, A. S., Eipper, B. A., Mains, R. E., and Amzel, L. M. (1997) *Science 278*, 1300−1305.
46. Viles, J. H., Cohen, F. E., Prusiner, S. B., Goodin, D. B., Wright, P. E., and Dyson, H. J. (1999) *Proc. Natl. Acad. Sci. U.S.A. 96*, 2042−2047.
47. Miura, T., Hori-i, A., and Takeuchi, H. (1996) *FEBS Lett. 396*, 248−252.
48. Stockel, J., Safar, J., Wallace, A. C., Cohen, F. E., and Prusiner, S. B. (1998) *Biochemistry 37*, 7185−7193.
49. Miura, T., Hori-i, A., Mototani, H., and Takeuchi, H. (1999) *Biochemistry 38*, 11560−11569.
50. Aronoff-Spencer, E., Burns, C. S., Avdievich, N. I., Gerfen, G. J., Peisach, J., Antholine, W. E., Ball, H. L., Cohen, F. E., Prusiner, S. B., and Millhauser, G. L. (2000) *Biochemistry 39*, 13760−13771.
51. Salmona, M., Malesani, P., De Gioia, L., Gorla, S., Bruschi, M., Molinari, A., Della Vedova, F., Pedrotti, B., Marrari, M. A., Awan, T., Bugiani, O., Forloni, G., and Tagliavini, F. (1999) *Biochem. J. 342*, 207−214.
52. Nguyen, J., Baldwin, M. A., Cohen, F. E., and Prusiner, S. B. (1995) *Biochemistry 34*, 4186−4192.
53. Cuajungco, M. P., Goldstein, L. E., Nunomura, A., Smith, M. A., Lim, J. T., Atwood, C. S., Huang, X., Farrag, Y. W., Perry, G., and Bush, A. I. (2000) *J. Biol. Chem. 275*, 19439−19442.
54. Westaway, D., and Prusiner, S. B. (1986) *Nucleic Acids Res. 14*, 2035−2044.

BI0029088